Journal of the Mechanics and Physics of Solids 122 (2019) 116–125

Contents lists available at ScienceDirect

Journal of the Mechanics and Physics of Solids

journal homepage: www.elsevier.com/locate/jmps

The transition from steady frictional sliding to inertia-dominated instability with rate and state friction

Kyungjae Im[a,*], Chris Marone[b], Derek Elsworth[a,b]

[a] Department of Energy and Mineral Engineering, EMS Energy Institute, and G3 Center, The Pennsylvania State University, University Park, PA 16802, United States

[b] Department of Geosciences, EMS Energy Institute, and G3 Center, The Pennsylvania State University, University Park, PA 16802, United States

ARTICLE INFO

Article history:
Received 8 June 2018
Revised 9 August 2018
Accepted 31 August 2018
Available online 5 September 2018

ABSTRACT

Unstable frictional slip motions are investigated with a rate and state friction law across the transitions from stable, quasi–static slip to dynamic, stick–slip motion, and finally to, inertia dominated quasi–harmonic vibration. We use a novel numerical method to capture the full dynamics and investigate the roles of inertial and quasistatic factors of the critical stiffness defining the transition to instability, K_c. Our simulations confirm theoretical estimates of K_c, which is dependent on mass and velocity. Furthermore, we show that unstable slip motion has two distinct dynamic regimes with characteristic limit cycles: (i) stick–slip motions in the quasi–static (slowly loaded) regime and (ii) quasi–harmonic oscillations in the dynamic (rapidly loaded) regime. Simulation results show that the regimes are divided by the dynamic frictional instability coefficient, $\eta = MV^2/\sigma aD_c$ and stiffness of the system K. The quasi–static regime is governed by the ratio K/K_c and both the period and magnitude of stick–slip cycles decrease with increasing loading rate. In the dynamic regime, slip occurs in harmonic limit cycles, the frequency of which increases with loading velocity to a limit set by the natural frequency of the system. Our results illuminate the origin of the broad spectrum of slip behaviors observed for systems ranging from manufacturing equipment to automobiles and tectonic faults, with particular focus on the role of elasto–frictional coupling in dictating the transition from slow slip to dynamic instability. We highlight distinct characteristics of friction–induced slip motions (stick–slip and friction–induced vibration) and show that the dynamic frictional instability coefficient (η) is a key parameter that both defines the potential for instability and determines the dynamic characteristics of instability.

1. Introduction

Friction plays a key role in the mechanical behavior of systems that involve slipping contacts. In many situations, the transition from stable to unstable slip motion is of primary interest. When such systems are loaded slowly, frictional motion often occurs as repeated episodes of quasi–stationary contact followed by rapid slip, which defines the classical 'stick–slip' instability (Bridgman, 1936, 1951; Rabinowicz, 1951, 1956; Singh, 1960; Shimamoto et al., 1980; Baumberger et al., 1994).

* Corresponding author.
E-mail addresses: kxi123@psu.edu (K. Im), marone@psu.edu (C. Marone), elsworth@psu.edu (D. Elsworth).

https://doi.org/10.1016/j.jmps.2018.08.026
0022-5096/

When loading is more rapid, frictional motion often occurs as a high frequency quasi–harmonic oscillation (Brockley and Ko, 1970), which is referred to as friction–induced vibration. The stick–slip instability has been analyzed intensely in earthquake science as it is directly analogous to natural earthquakes (Brace and Byerlee, 1966) as well as in slowly loaded mechanical systems (Kammer et al., 2014, 2015; Svetlizky et al., 2017). Friction induced vibration has also received much attention, because of its importance in engineering systems where it causes surface wear, damage and noise (Ibrahim, 1994). However, the transition from stick–slip to frictional vibration has received less attention, despite its importance in engineered and natural systems.

The conditions for the stability transition from stable to unstable sliding with rate and state friction are presented by Rice and Ruina (1983). They showed that stable sliding at a certain velocity can only be achieved when system stiffness is larger than a critical value K_c. The parameter K_c represents a critical rate of frictional weakening with slip. Notably, K_c depends not only on friction parameters, but also on dynamic variables, i.e., mass and velocity (Ruina, 1983; Rice and Ruina, 1983; Gu et al., 1984; Rice, 1993; Baumberger and Caroli, 2006; Ranjith and Rice, 1999; Rice et al., 2001; Perfettini and Molinari, 2017). This analysis shows that a system can become significantly unstable with increased mass and slip velocity, indicating that dynamic (inertial) factors are key parameters controlling slip stability in the high velocity slip regime.

Modern constitutive laws for sliding recognize the importance of frictional slip rate and past states of the sliding surfaces. These effects form the basis for the rate and state friction constitutive laws (Dieterich, 1979a, b; Runia, 1983; Rice and Ruina, 1983), which have been applied to a wide range of systems ranging from tectonic faults (Scholz, 2002; Luo and Ampuero, 2018; van den Ende et al., 2018) to nanoscale, atomic contacts (e.g., Tian et al., 2017). Rate and state friction (RSF) laws successfully capture laboratory observations of macroscopic friction for a range of loading rates (Marone, 1998a; Baumberger and Caroli, 2006). The laws were originally developed to describe frictional behavior in rock (Dieterich, 1979a; Ruina, 1983), but later it was shown that they are applicable to wide variety of materials (Dieterich and Kilgore 1994, Heslot et al., 1994; Baumberger and Caroli, 2006).

For frictional systems that are loaded slowly, both analytic and laboratory observations of stick–slip magnitude show a strong inverse relationship with the logarithm of loading rate (i.e. magnitude decreases with increased velocity) (Gu and Wong 1991; Karner and Marone, 2000; Mair et al., 2002; Beeler et al., 2001, 2014; Scuderi et al., 2015). One may expect that the magnitude of stick–slip will decrease continuously with increased velocity. However, this expectation is at odds with the stability analysis of Rice and Ruina (1983), which predicts that slip will become unstable at high slip velocity. One may assume a smooth transition from the quasi–static (low velocity) regime to the dynamic (high velocity) regime. However, the dynamic regime for systems exhibiting rate and state friction has received relatively little attention (cf., Rice, 1993), with few works focused on complete solutions that account for the transition from stable sliding to fully dynamic motion with inertia.

Here, we use a novel numerical solution to address the full spectrum of slip modes for a system with rate and state friction and 1D elastic coupling (Im et al., 2017). We focus on numerical observations of dynamic friction behavior throughout the transition from quasi–static to dynamic motion. We investigate frictional behaviors of (i) the stable to unstable transition induced by dynamic effects and (ii) dynamic characteristics of frictional slip throughout the transition from quasi–static (slow loading) to dynamic loading.

2. Background summary

2.1. Rate and state friction law

In the framework of RSF, frictional resistance is dependent on slip velocity V and the history of sliding, which is characterized in terms of a state variable θ (Dieterich, 1979a; Ruina, 1983). The most widely used form is:

$$\mu = \mu_0 + \alpha \ln\left(\frac{V}{V_0}\right) + b \ln\left(\frac{V_0\theta}{D_c}\right) \tag{1}$$

where μ_0 is a reference friction coefficient that corresponds to steady state friction at reference slip velocity V_0, D_c is a critical slip distance that characterizes the evolution of friction following a perturbation, and the non-dimensional parameters a and b represent the magnitude of the direct change in friction following a change in slip velocity and the subsequent evolution of friction.

The evolution of friction following a perturbation imposed during steady sliding is modulated by time via contact aging processes and slip. Although a multitude of processes may affect friction evolution, two evolution laws have received the most attention (Marone, 1998a). The Dieterich (or aging) law focuses on the evolution of state with time:

$$\frac{d\theta}{dt} = 1 - \frac{V\theta}{D_c} \tag{2}$$

whereas the Ruina (or slip) law characterizes friction evolution strictly in terms of the sliding distance. For the Ruina law, the rate of state evolution vanishes as velocity goes to zero:

$$\frac{d\theta}{dt} = -\frac{V\theta}{D_c} \ln\left(\frac{V\theta}{D_c}\right) \tag{3}$$

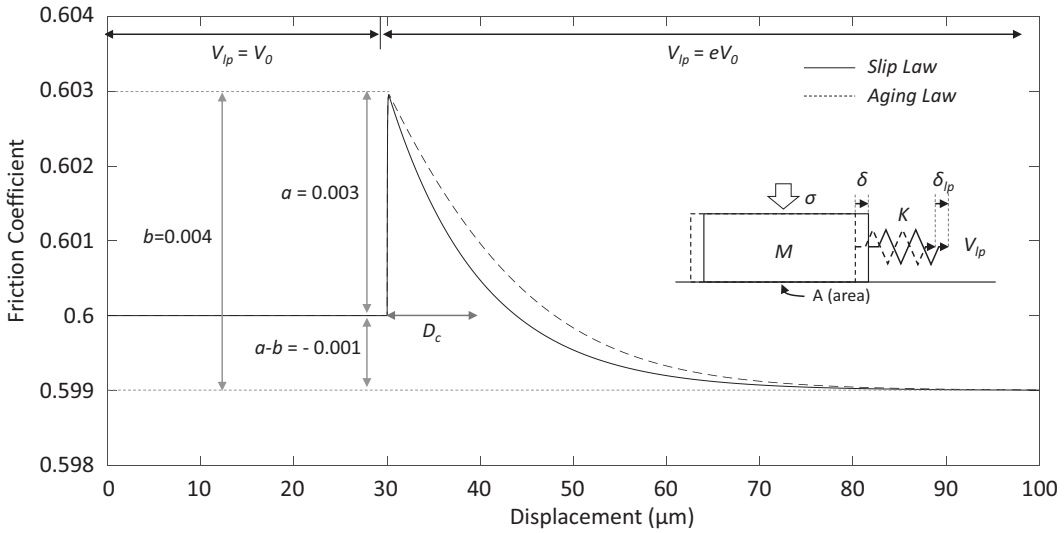

Fig. 1. Friction response to an *e*-fold velocity step for a stiff ($\delta \approx \delta_{lp}$) spring-slider system undergoing quasi–static ($M = 0$) motion. Results are shown for both the Ruina (slip) and Dieterich (aging) state evolution laws. RSF parameters are: $a = 0.003$, $b = 0.004$, $D_c = 10\,\mu m$, $V_0 = 30\,\mu m/s$ and normalized stiffness $K/\sigma = 1 \times 10^5/m$. Inset shows spring-slider system. Gravitational force is included in σ.

The two evolution laws behave similarly for small perturbations around steady state ($\theta \sim D_c/V$) but they diverge substantially when velocity is far from steady state (Ampuero and Rubin, 2008; Bhattacharya et al., 2015, 2017).

2.2. Elastic coupling

In a frictional system with one dimensional elastic interaction, the force balance governing motion is

$$\frac{M\ddot{\delta}}{\sigma} = \frac{K(\delta_{lp} - \delta)}{\sigma} - \mu \tag{4}$$

where M is mass per unit area (kg/m^2), K is a stiffness expressed in units of shear stress (Pa/m), and σ is normal stress (see Fig. 1 inset). Note that the force balance is divided by contact area and normal stress in Eq. (4), which shows that normalized shear stress (first term on the RHS) and friction (μ) decouple when the inertial term (LHS) is significant. For a system where the mechanical response is stiff ($\delta \approx \delta_{lp}$) and motion is quasi–static ($M \approx 0$), the RSF response to an e-fold increase in slip velocity can be illustrated according to Eqs. (1)–(3). For a sudden jump in velocity by a factor of e, friction increases immediately by a magnitude corresponding to a (direct effect) and then decays by a magnitude corresponding to b (evolution effect) over an e-folding slip distance given by D_c (Fig. 1). After sufficient slip, friction reaches a new steady state. The difference in steady state friction between the original slip rate V_o and the new slip rate V is given by $(a - b)\ln(V/V_0)$.

2.3. Critical stiffness and stability criterion

Fig. 1 implies that unstable sliding may occur when $(a - b) < 0$, because frictional resistance decreases with increased velocity and this may induce self-driven acceleration. Several studies have shown that this condition is indeed necessary for unstable slip but not sufficient (Runia, 1983; Rice and Ruina, 1983; Rice, 1993; Ranjith and Rice, 1999). Steady sliding at velocity V occurs when the elastic stiffness K is larger than the critical stiffness K_c:

$$K_c = -\frac{V d\tau_{ss}(V)/dV}{D_c}\left[1 + \frac{MV}{D_c \partial \tau(V,\theta)/\partial V}\right] \tag{5}$$

where τ is shear stress and $\tau_{ss}(V)$ is the steady state shear stress at velocity V (Rice and Ruina, 1983). Eq. (5) is general and not strongly restricted to RSF. For a one state variable RSF law, Eq. (5) can be further simplified to (Gu et al., 1984; Roy and Marone, 1996; Baumberger and Caroli, 2006),

$$K_c = \frac{(b-a)\sigma}{D_c}\left[1 + \frac{MV^2}{\sigma a D_c}\right] \tag{6}$$

For quasi–static motion, Eq. (6) can be simplified by substituting $M = 0$, i.e. $K_{c,qs} = (b-a)\sigma/D_c$ (Ruina, 1983). These relations show that velocity weakening, $(a - b) < 0$, is required for frictional instability, because if K_c is negative, only stable

sliding is possible given that K is positive. The value of K_c dictates the potential for frictional instability for a sliding system. As K_c increases, higher system stiffness is required for stable sliding.

The second bracketed term in Eq. (6) is a dimensionless number representing a "dynamic" effect. Given its importance for slip stability and the transition from stick-slip to frictional vibration, we define the dynamic frictional instability coefficient η

$$\eta = \frac{MV^2}{\sigma a D_c} \tag{7}$$

The parameter η represents the dynamic contribution to frictional instability and can be compared to the purely quasi–static factor. Eq. (6) shows that mass M and velocity V play a key role in frictional motion. The dynamic effect on K_c can be negligible at slow velocity ($V^2 << \sigma a D_c/M$), but it can be significant when mass and velocity are high and $\eta \geq 1$, which represents the value at which the dynamic effect exceeds the quasi–static effect on K_c. Note that η can increase without limit and is strongly sensitive to slip velocity ($\eta \sim V^2$), indicating that any system with $a - b < 0$ has potential for unstable sliding at sufficiently large velocity.

3. Simulation results

The simulations are conducted using a recent solution that provides increased numerical stability over the full range of deformational modes - from stable sliding to fully dynamic, unstable motion (Im et al., 2017). In this method, RSF and velocity are solved for each numerical step as constrained within the solution imposed by force balance. The time-discretized equation for displacement is

$$\delta^{i+1} = [\delta^i - ({\delta_{lp}}^{i+1} - \mu^{i+1}\sigma/K)]cos(\omega\Delta t) + \frac{V^i}{\omega}\sin(\omega\Delta t) + ({\delta_{lp}}^{i+1} - \mu^{i+1}\sigma/K) \tag{8}$$

where superscripts i and $i+1$ denote successive time steps and ω is angular velocity defined as $\omega = \sqrt{K/M}$. Using the midpoint velocity, we define

$$V^{i+1} = 2\frac{(\delta^{i+1} - \delta^i)}{\Delta t} - V^i \tag{9}$$

Rate and state friction at each numerical step is calculated using V^{i+1} and simultaneously solved with Eqs. (8) and (9) (see Im et al. (2017) for details).

We conducted two sets of numerical experiments. The first set is conducted for $K > K_{c,qs}$. According to Eq. (6), this condition yields stable sliding at slowly slipping motion while it can become unstable at sufficiently fast velocity. Our second set of numerical experiments are conducted with $K < K_{c,qs}$, which always yields unstable slip motion regardless of the slip velocity. It is well known that this condition yields stick–slip instability when the system is loaded slowly (Rice and Tse, 1986; Im et al., 2017). Here, we go beyond the earlier work and study the full range from slow to fast loading velocity, spanning this transitional area with a single solution method, including cases where the dynamic effect becomes significant ($\eta > 1$).

3.1. Velocity stepping over stable/unstable boundary

For a constant elastic stiffness K, Eq. (6) defines a critical velocity V_c as,

$$V_c = \sqrt{\frac{\sigma a D_c}{M}\left(\frac{KD_c}{(b-a)\sigma} - 1\right)} \tag{10}$$

The critical velocity represents a stability condition, such that for loading at subcritical rates ($V_{lp} < V_c$), friction will be eventually stabilized at the loading velocity. Conversely, if the system is loaded at supercritical velocities ($V_{lp} > V_c$), slip will be unstable.

We conducted numerical simulations of the frictional response to step changes in loading velocity using sub- and supercritical velocity steps (Fig. 2). RSF parameters were fixed at $\mu_0 = 0.6$, $V_0 = 10^{-9}$ m/s, $D_c = 10\,\mu$m, $a = 0.003$ and $b = 0.006$ which roughly typify polished granite surfaces or shear within granular layers used to simulate the wear and breccia (fault gouge) found in tectonic fault zones (Marone, 1998a). We used $\sigma = 2$ MPa, $M = 3000$ kg/m^2 and an elastic stiffness K of $1.5K_{c,qs}$ ($K = 900$ MPa/m; $K_{c,qs} = 600$ MPa/m). For these parameters Eq. (10) yields a critical velocity V_c of ~3.16 mm/s. Our simulations begin with stable sliding at an initial velocity $V = 0.1$ mm/s, which is well below V_c, and then step changes in loading velocity V_{lp} are imposed using three values (Fig. 2) that correspond to: (i) strongly subcritical velocity (0.3 mm/s), (ii) slightly subcritical velocity (3.1 mm/s) and (iii) slightly supercritical velocity (3.2 mm/s). Fig. 2b shows the dynamic critical stiffness (Eq. (6)) for each case along with the elastic stiffness K. The stability transition is predicted to occur between $V_{lp} = 3.1$ and 3.2 mm/s, corresponding to $V_c \sim 3.16$ mm/s (Fig. 2b).

The friction responses for the three cases studied (Fig. 2a) clearly demonstrate that sliding stability is indeed determined by the "dynamic" critical stiffness, consistent with Eq. (6). All three cases show initially unstable oscillations immediately following the velocity jump, showing that the stable systems can become unstable with sudden velocity increase

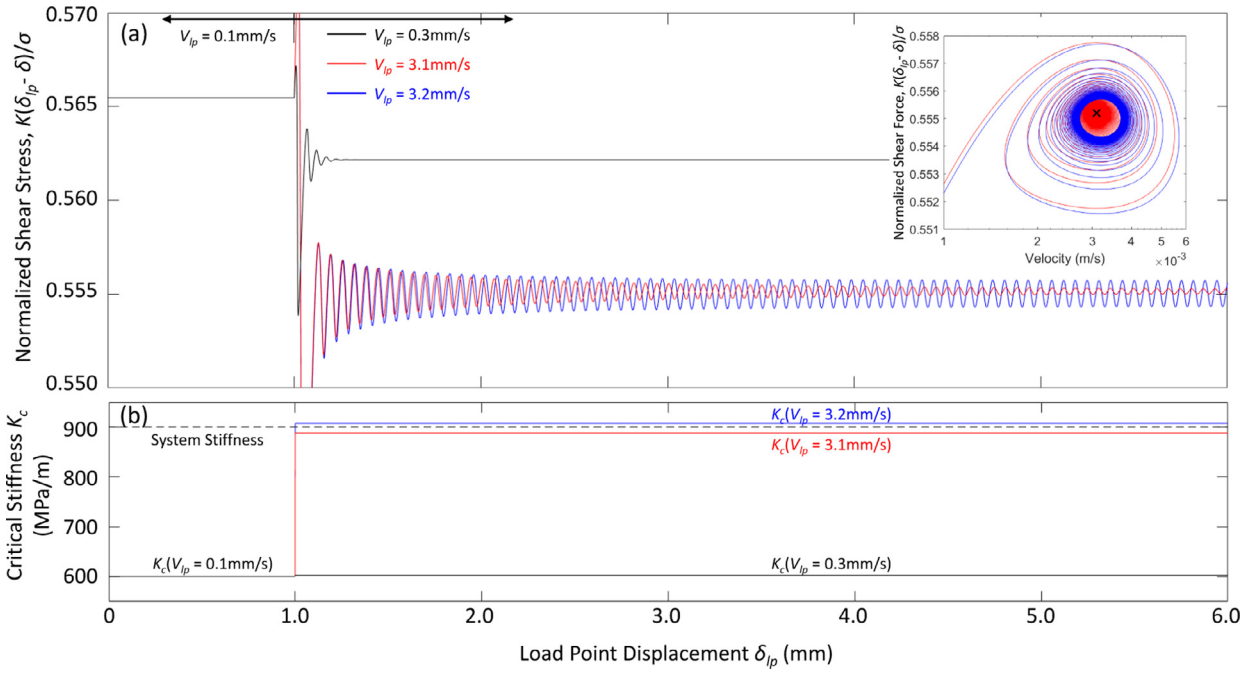

Fig. 2. (a): Friction response to three velocity steps: (i) strongly subcritical velocity (0.3 mm/s; black), (ii) slightly subcritical velocity (3.1 mm/s; red) and (iii) slightly supercritical velocity (3.2 mm/s; blue). Simulations used the Ruina law with $\mu_0 = 0.6$, $V_0 = 10^{-9}$ m/s, $D_c = 10\,\mu$m, $a = 0.003$, $b = 0.006$, $\sigma = 2$ MPa and $M = 3000$ kg/m^2 with stiffness K set to 1.5 of the quasi–state critical stiffness ($K = 900$ MPa/m; $K_{c,qs} = 600$ MPa). These input parameters yield a critical velocity of 3.16 mm/s. Note that the subcritical velocity step (red) converges to the predicted value of slip velocity (marked with an $\times$ on the phase diagram, inset to panel a) while the supercritical velocity case (blue) results in a limit cycle oscillation. (b) Calculated critical stiffness for each case (colors correspond to those of panel a) with system stiffness also shown (black dashed line). The identical simulation results for the Dieterich law are presented in the supplement. (For interpretation of the references to colour in this figure legend, the reader is referred to the web version of this article.)

(Gu et al., 1984). However, their subsequent behaviors are significantly different (Fig. 2a). For the strongly subcritical case (black line; $V_{lp} = 0.3$ mm/s), the oscillation rapidly attenuates and sliding quickly becomes steady at the new loading velocity. For the two higher loading rate cases, the initial response involves a large stress drop and rapid acceleration. Slip velocity oscillates to a large magnitude and gradually decreases to steady sliding for the jump to 3.1 mm/s, whereas the jump to 3.2 mm/s produces sustained harmonic oscillations that range from ~2.6 to 4 mm/s (Fig. 2a inset).

The convergence behaviors of the two near critical cases are compared in the phase plane diagram (Fig. 2a) for an extended duration of 10 s after the velocity steps. Note that the two cases are initially similar but that their final behaviors are significantly different. The oscillation for the subcritical case (red line) converges to its theoretical steady state point (marked by the $\times$ in the inset to Fig. 2a), while the supercritical case converges to a periodic limit cycle.

We conducted multiple simulations to further examine the transition from stable to unstable motion (Fig. 3). We used the same set of RSF parameters as above (Fig. 2) while varying the mass and velocity. We tested 12 values of M and 13 velocities, for a total of 156 cases. Fig. 3 shows results in terms of the magnitude of the normalized shear stress oscillation for the limit cycle (e.g., Fig. 2a). The boundary between stable (empty circles) and unstable (filled circles) motion corresponds to the prediction of the Rice-Ruina dynamic stability criteria (red dashed line; Eq. (10)).

3.2. Dynamic characteristics of instability

The periodic limit cycles demonstrated in Fig. 2a are clearly not a stick-slip instability, but rather represent a harmonic oscillation. As stick–slip instabilities at slow loading rates are well documented with rate and state friction (Rice and Tse, 1986; Im et al., 2017), these observations show that the two different dynamical frictional regimes (stick–slip and harmonic vibration) can be integrated within a single framework of frictional response, provided inertia is correctly incorporated. The quasi-harmonic oscillations we observe (Fig. 2) can be understood *via* the inertial term of the force balance ($M\ddot{\delta} = K(\delta_{lp} - \delta)$) and therefore should be related to the dynamic frictional instability coefficient, η.

We studied a suite of cases to illustrate how limit-cycles vary with loading velocity and dynamical parameters and summarize results using the magnitude of the limit cycle oscillation (Fig. 4). The simulations of Fig. 4 are conducted with the Ruina law (see supplement for Dieterich Law results) and $a = 0.005$, $b = 0.008$, $D_c = 10\,\mu$m and $\sigma = 4$ MPa, which yields $K_{c,qs} = 1.2$ GPa/m. We used elastic stiffness $K = 0.96$ GPa/m (black) and $K = 0.60$ GPa/m (gray) that yield $K = 0.8K_{c,qs}$ and $K = 0.5$ $K_{c,qs}$ respectively. Thus, the systems always yield unstable motion regardless of mass or velocity (Figs 4b and c). We varied

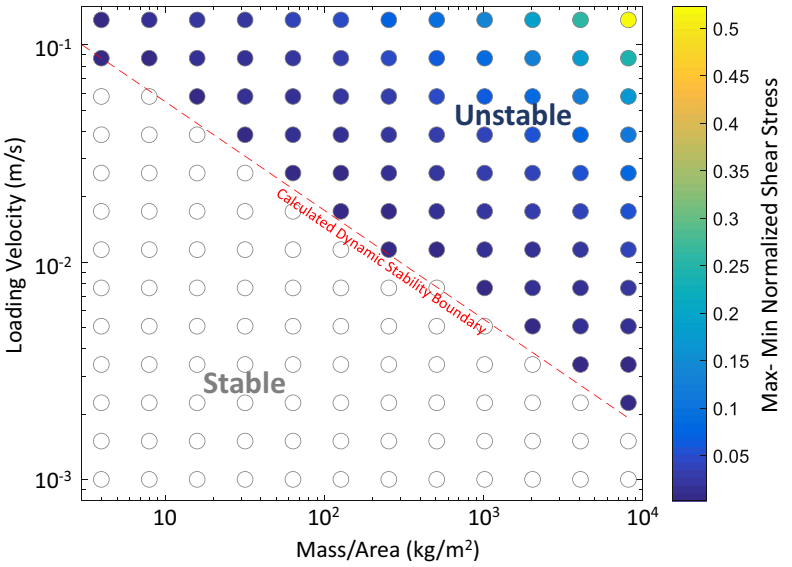

Fig. 3. Magnitudes of the normalized shear stress oscillation at the limit cycle (10 s after velocity step) for 12 values of M and 13 loading velocities V_{lp}. Input parameters are identical to simulations in Fig. 2 except M and V_{lp}. Empty circles denotes stable frictional motion. Red dashed line shows that the Rice-Ruina dynamic stability criterion predicts our results.

loading velocity across five orders of magnitude using a constant value of mass per unit area $M = 100\,\mathrm{kg/m^2}$. All simulations converged to periodic limit cycles.

Our results define two distinct regimes, with stick-slip motion occurring for loading velocities below a critical value and harmonic oscillations occurring above (Fig. 4). For slower loading rates, the oscillation magnitude decreases roughly log-linearly with V_{lp}, which is a well-documented behavior of stick–slip friction drop (Karner and Marone, 2000; Beeler et al., 2001, 2014; Ben-David et al., 2010; He et al., 2003, Tian et al., 2017). One way to understand this is to consider that peak friction increases with contact age, which scales inversely with stick–slip recurrence interval (Marone, 1998b). Our results also show that the trend of decreasing stick–slip magnitude with loading rate becomes nonlinear, with stick–slip stress drop reaching a minimum at loading velocities of ~3–5 cm/s, depending on stiffness K (Fig. 4). With increased loading velocity, the magnitude of harmonic oscillations increases with loading rate, which defines the dynamic regime.

The transition from quasi–static stick–slip to quasi harmonic oscillations can be described by the emergence of dynamic instability coefficient η. Fig. 4a shows that the oscillation magnitude begins to deviate from the linear trend when the dynamic instability coefficient (blue line) starts to increase. In fact, it is expected that the decreasing trend of stress drop in the quasi–static regime does not extend to zero, because the elastic stiffness for stable sliding increases strongly as loading rate increases, due to the dynamic effects included in η. Note that η is negligible at low velocity ($V^2 << \sigma a D_c/M$), however once it reaches a value of ~ 1, it increases rapidly, as the square of velocity.

The dynamic characteristics of frictional instability show clear differences between the two regimes illustrated in Fig. 4. In the quasi–static regime, the stick–slip limit cycle is apparent (Fig. 4b). Conversely in the dynamic regime, friction exhibits a high frequency quasi–harmonic oscillation (Fig. 4c) similar to what we saw in Fig. 2.

It is clear that inertia plays a key role in distinguishing the two regimes. In Fig. 4b and c, the gap between normalized shear stress (black line; first term of RHS Eq. (4)) and rate and state friction (red dashed line; second term of RHS Eq. (4)) is a direct consequence of inertia; in particular the magnitude of the normalized inertial force (LHS of Eq. (4)). During stick–slip motion (Fig. 4b), the inertial term is apparent only in the short dynamic slip phase (see inset Fig. 4b). Conversely, inertia is significant throughout the limit cycles observed during quasi–harmonic oscillations (Fig. 4c).

It is also instructive to evaluate the two frictional instability regimes in terms of event frequency (Fig. 5). Note the similarity to Fig. 4a, which is expected given that an increase in loading rate results in an increase in event frequency. The log-linear relation between shear stress drop (magnitude) and frequency (or recurrence time) also appears in the quasi–static regime, showing that a larger magnitude of friction drop is associated with a longer duration of recurrence time. This behavior is well documented analytically, in lab data, and for natural earthquake cycles (Vidale et al., 1994; Marone et al., 1995; McLaskey et al., 2012; Beeler et al., 2001, 2014; Im et al., 2017). For higher frequency oscillations, the event magnitude reaches a minimum and increases significantly as loading rate increases (Fig. 5). However, our results indicate that the increase in event frequency is limited by the natural frequency of the system ($f_n = (1/2\pi)\sqrt{K/M}$), which is 493 Hz for $K = 0.96$ GPa and 390 Hz for $K = 0.60$ GPa in these simulations (vertical red lines; $M = 100\,\mathrm{kg/m^2}$).

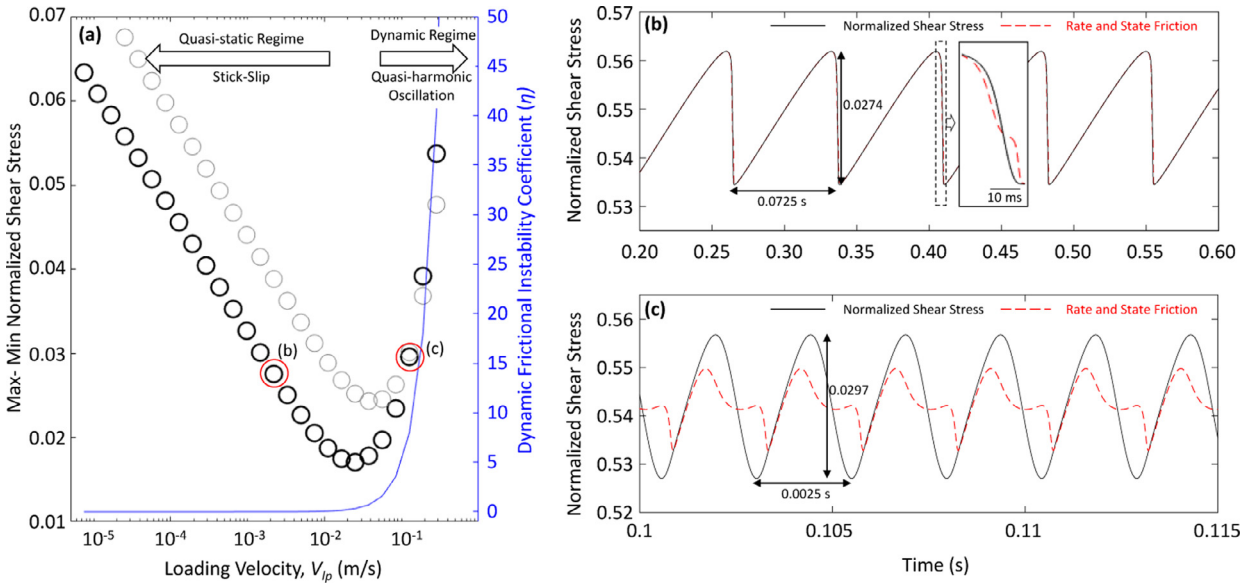

Fig. 4. (a) Magnitude of friction limit cycles during stick–slip and harmonic oscillations for a range of loading velocities. We used the Ruina law with $a=0.005$, $b=0.008$, $D_c=10\,\mu m$, $\sigma=4\,MPa$ and $M=100\,kg/m^2$ with $K=0.96\,GPa/m$ (black) and $K=0.60\,GPa/m$ (gray). These input parameters yield $K=0.8\,K_{c,qs}$ and $K=0.5\,K_{c,qs}$ and therefore result in unstable motion regardless of the loading velocity. Panel (a) defines two distinct regimes: stick–slip sliding with quasi–static slip rates and dynamic motion defined by harmonic oscillations. The emergence of the dynamic regime coincides with the instability coefficient η (blue line) becoming ≥ 1. Panels (b) and (c) show examples of friction in each regime, stick–slip in (b) and quasi-harmonic oscillation in (c). Red and black curves represent normalized shear stress and rate and state friction, respectively. According to the force balance (Eq. (4)), the gap between the black (normalized shear stress) and red (friction) curves represents the effect of inertia. In the stick-slip regime, inertia is only apparent during a short period of dynamic slip (panel (b) inset) whereas it is always significant in the dynamic regime of (c). Identical simulations with the Dieterich law are presented in the supplement. (For interpretation of the references to colour in this figure legend, the reader is referred to the web version of this article.)

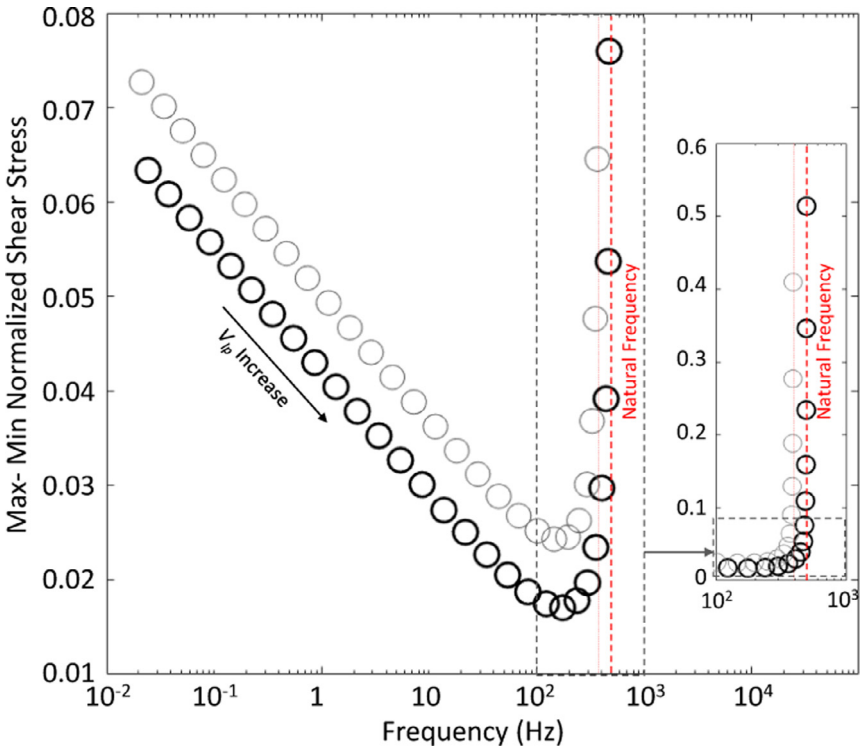

Fig. 5. Max-min normalized shear stress vs. frequency at limit cycle with identical simulation results to Fig. 4. Frequency generally increases with V_{lp}. However, frequency increases are limited at the natural frequency f_n (493 Hz for black and 390 Hz for gray) of the system. Extended simulation results to a larger loading rate are presented in inset, confirming that same limit is applied at the larger loading rates.

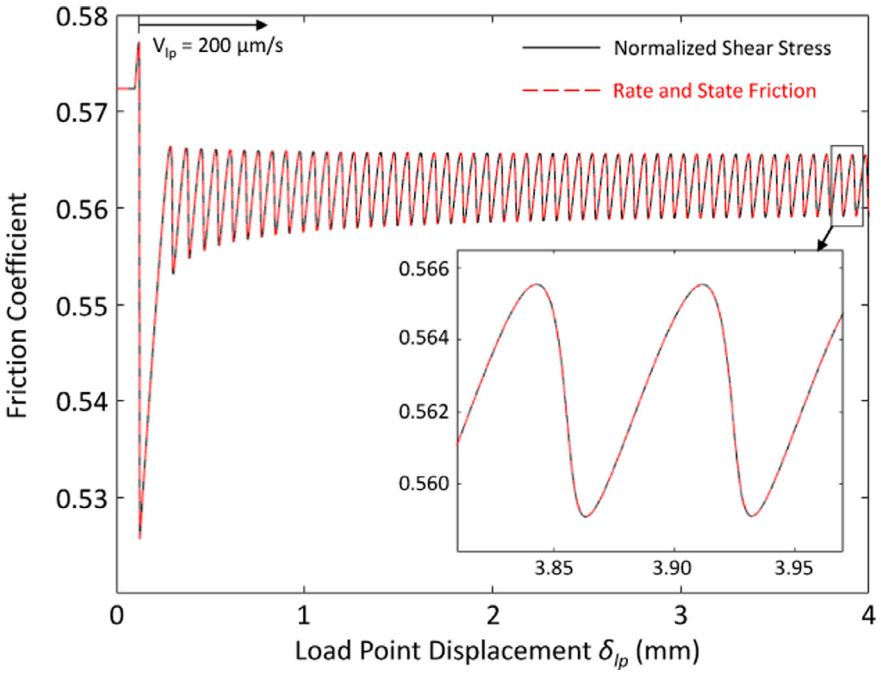

Fig. 6. Friction response for velocity steps from 10 μm/s to 200 μm/s at load point displacement 0.1 mm. Frictional parameters, mass and normal stress are identical to the simulation in Fig. 2, but stiffness K is set to 1.0005 $K_{c,qs}$ to prompt an instability transition with only a slight increase is η. The dynamic frictional instability coefficient at 200 μm/s is $\eta = 0.002$. Black line denotes normalized shear stress and red dashed line denotes rate and state friction. Note that the black line and red dashed lines almost fully overlap. (For interpretation of the references to colour in this figure legend, the reader is referred to the web version of this article.)

4. Discussion

4.1. Slow stick–slip at $K \sim K_c$

We find that a quasi–harmonic oscillation emerges when $K < K_c$ and η is significant. Here we conduct a stable to unstable velocity stepping simulation similar to that in Fig. 2, but with only a small increase of η to observe the characteristics of friction with $K < K_c$ but where η is insignificant. We used identical friction parameters to the simulations in Fig. 2, but the loading velocity is increased from 10 μm/s to 200 μm/s - yielding $\eta = 0.002$ at $V_{lp} = 200$ μm/s. To achieve a stable to unstable transition for the given η, the stiffness of the system is set only slightly larger than the quasi–static critical stiffness ($K = 1.0005 K_{c,qs}$) so that the stiffness become slightly smaller than the dynamic critical stiffness at $V = 200$ μm/s ($K = 0.9985 K_c$).

The resulting friction is shown in Fig. 6, representing a stable – unstable transition at the loading velocity jump. The normalized shear stress (black line) and rate and state friction (red dashed line) almost fully overlap, representing that the inertial effect ($M\ddot{\delta}/\sigma$ in Eq. (4)) is insignificant. A zoomed-in plot (Fig. 6 inset) shows that the inertial effect is still insignificant even in the friction drop phase. This characteristic is inconsistent with general stick–slip motion which shows significant decoupling of normalized shear stress and friction at the friction drop (Fig. 4b and insets). Apparently the "slip" phase in Fig. 6 is much slower than that of stick–slip (Fig. 4b). In fact, this slow stick–slip motion at $K \sim K_c$ has been recognized in quasi–static (no inertia consideration) numerical simulations (e.g., Ruina, 1983) and, more recently, with experimental observation over a wide range of critical stiffnesses (Leeman et al., 2016). Fig. 6 shows that slow stick–slip also emerges even with full consideration of inertia, and the inertial effect remains insignificant throughout the whole process.

4.2. Potential for frictional instability

The potential for the emergence of a dynamic instability increases significantly with slip velocity. Our analysis indicates that friction-induced vibration (harmonic oscillation) can potentially emerge in any system exhibiting velocity weakening friction ($a - b < 0$). The emergence of unstable sliding merely requires a sufficiently high slip velocity ($V > V_c$). Moreover, since the critical stiffness (or dynamic frictional instability coefficient η) increases with V^2, this velocity requirement can be easily met in fast slipping contacts such as those in mechanical parts for example, vehicle brake system. The potential for this emergence of instability can be decreased by reducing mass (η decrease) which, at the same time, will increase oscillation frequency once emerged.

The dynamic frictional instability coefficient (η) not only represents the potential for the emergence of frictional instability but also determines the instability regime. There is no clear boundary between the regimes presented in these simulations as transition from stick-slip to quasi-harmonic oscillation occurs gradually and it is also dependent on the stiffness of the system. However, one may use $\eta = 1$ to characterize instability regimes as suggested by Roy and Marone (1996), since it denotes the state where quasi–static and dynamic effects are identical and after this point, η increases rapidly with velocity. With the input parameters of the simulation in Fig. 4, this is at $V = 4.47 \times 10^{-2}$ m/s which corresponds well with our transition zone.

4.3. Dynamic instability in natural fault system

Quasi–harmonic oscillations can also be observed in natural fault slip, as, so called, harmonic tremor. Harmonic tremors are frequently observed where applied loading rate or slip rate on the fault is temporarily increased, for example, by subsurface magma transfer (volcanic tremor) (Choudt, 1996; Dmitrieva et al., 2013) or by injection-induced slip (Das and Zoback, 2013; Derode et al., 2015). In both cases, the fault contacts are forced to slip under continuous loading at increased velocity. This condition should significantly enhance the dynamic frictional instability coefficient ($MV^2/\sigma aD_c$), and may result in quasi–harmonic oscillation on the fault.

5. Conclusions

We show that frictional stability on high velocity slipping contacts is indeed controlled by inertia and related to dynamic effects. Furthermore, we observe that these dynamic effects determine the dynamic characteristics of the resulting unstable slip motions: stick–slip and quasi–harmonic oscillation. Magnitudes of shear stress oscillations decrease with increased velocity in the quasi–harmonic (stick–slip) regime while, it significantly increases with velocity in the dynamic (quasi–harmonic oscillation) regime. Frequency increases with increased velocity but there exists a frequency limit at the natural frequency of the system. Dynamic frictional instability coefficient ($\eta = MV^2/\sigma aD_c$) is a key parameter that defines the potential for dynamic instability and determines the dynamic characteristics of unstable slip motions.

Acknowledgments

This work is a partial result of support from the U.S. Department of Energy under projects DE-FE0023354 and DE_EE0006762 and the U.S. National Science Foundation under projects EAR-1520760 and EAR-1547441. This support is gratefully acknowledged.

Supplementary materials

Supplementary data associated with this article can be found, in the online version, at 10.1016/j.jmps.2018.08.026.

References

Ampuero, J.P., Rubin, A.M., 2008. Earthquake nucleation on rate and state faults – aging and slip laws. J. Geophys. Res. 113, B01302. doi:10.1029/2007JB005082.

Baumberger, T., Caroli, C., 2006. Solid friction from stick–slip down to pinning and aging. Adv. Phys. 55 (3–4), 279–348. https://doi.org/10.1080/00018730600732186.

Baumberger, T., Heslot, F., Perrin, B., 1994. Crossover from creep to inertial motion in friction dynamics. Nature 367, 544–546.

Bhattacharya, P., Rubin, A.M., Bayart, E., Savage, H.M., Marone, C., 2015. Critical evaluation of state evolution laws in rate and state friction: fitting large velocity steps in simulated fault gouge with time-, slip-, and stress-dependent constitutive laws. J. Geophys. Res. 120, 6365–6385. https://doi.org/10.1002/2015JB012437.

Bhattacharya, P., Rubin, A.M., Beeler, N.M., 2017. Does fault strengthening in laboratory rock friction experiments really depend primarily upon time and not slip? J. Geophys. Res. 122, 6389–6430. https://doi.org/10.1002/2017JB013936.

Beeler, N.M., Hickman, S.H., Wong, T.-f., 2001. Earthquake stress drop and laboratory-inferred interseismic strength recovery. J. Geophys. Res. 106 (B12), 30701–30713. https://doi.org/10.1029/2000JB900242.

Beeler, N.M., Tullis, T., Junger, J., Kilgore, B., Goldsby, D., 2014. Laboratory constraints on models of earthquake recurrence. J. Geophys. Res. 119 (12), 8770–8791. https://doi.org/10.1002/2014JB011184.

Ben-David, O., Rubinstein, S.M., Fineberg, J., 2010. Slip–stick and the evolution of frictional strength. Nature 463 (7277), 76–79. https://doi.org/10.1038/nature08676.

Brace, W.F., Byerlee, J.D., 1966. Stick–slip as a mechanism for earthquakes. Sci., V. 153, 990–992.

Bridgman, P.W., 1936. Shearing phenomena at high pressure of possible importance for geology. J. Geol. 44, 653–669.

Bridgman, P.W., 1951. Some implications for geophysics of high-pressure phenomena. Geol. Sot. Am, Bull. 62, 533–536.

Brockley, C.A., Ko, P.L., 1970. Quasi–harmonic friction–induced vibration. J. Lubr. Technol. 550–556.

Chouet, B.A., 1996. Long-period volcano seismicity: its source and use in eruption forecasting. Nature. https://doi.org/10.1038/380309a0.

Das, I., Zoback, M.D., 2013. Long-period long-duration seismic events during hydraulic stimulation of shale and tight-gas reservoirs — part 2: location and mechanisms. Geophysics 78 (6). KS109-KS117. https://doi.org/10.1190/geo2013-0165.1.

Derode, B., Guglielmi, Y., De Barros, L., Cappa, F., 2015. Seismic responses to fluid pressure perturbations in a slipping fault. Geophys. Res. Lett. 42 (9), 3197–3203. https://doi.org/10.1002/2015GL063671.

Dieterich, J.H., 1979a. Modeling of rock friction: 1. experimental results and constitutive equations. J. Geophys. Res. 84, 2161–2168.

Dieterich, J.H., 1979b. Modeling of rock friction: 2. simulation of preseismic slip. J. Geophys. Res. 84, 2169–2175.

Dieterich, J.H., Kilgore, B.D., 1994. Direct observation of frictional contacts: new insights for state-dependent properties. Pagoeph. 143 (1–3), 283–302. https://doi.org/10.1007/BF00874332.

Dmitrieva, K., Hotovec-Ellis, A.J., Prejean, S., Dunham, E.M., 2013. Frictional-faulting model for harmonic tremor before redoubt volcano eruptions. Nat. Geosci. 6 (8), 652–656. https://doi.org/10.1038/ngeo1879.
van den Ende, M.P.A., Chen, J., Ampuero, J.-P., Niemeijer, A.R., 2018. A comparison between rate-and-state friction and microphysical models, based on numerical simulations of fault slip. Tectonophysics 733, 273–295. https://doi.org/10.1016/J.TECTO.2017.11.040.
Gu, J.-C., Rice, J.R., Runia, A., Tse, S., 1984. Slip motion and stability of a single degree of freedom elastic system with rate and state dependent friction. J. Mech. Phys. Solids V 32, 167–196. doi:10.1016/S0022-5096(98)00113-6.
Gu, Y., Wong, T., 1991. Effects of loading velocity, stiffness, and inertia on the dynamics of a single degree of freedom spring-slider system. J. Geophys. Res. 96, 21677–21691. https://doi.org/10.1029/91JB02271.
He, C., Wong, T., Beeler, N.M., 2003. Scaling of stress drop with recurrence interval and loading velocity for laboratory-derived fault strength relations. J. Geophys. Res. 108 (B1), 2037. https://doi.org/10.1029/2002JB001890.
Heslot, F., Baumberger, T., Perrin, B., Caroli, B., Caroli, C., 1994. Creep, stick–slip and dry-friction dynamics: experiments and a heuristic model. Phys. Rev. E 49 (6).
Ibrahim, R.A., 1994. Friction-induced vibration, chatter, squeal, and chaos part I: mechanics of contact and friction. Appl. Mech. Rev. 47, 209–226.
Im, K., Elsworth, D., Marone, C., Leeman, J., 2017. The impact of frictional healing on stick–slip recurrence interval and stress drop: implications for earthquake scaling. J. Geophys. Res. https://doi.org/10.1002/2017JB014476.
Kammer, D.S., Yastrebov, VA, Anciaux, G, Molinari, JF, 2014. The existence of a critical length scale in regularised friction. J. Mech. Phys. Solids 63.
Kammer, DS, Radiguet, M, Ampuero, JP, Molinari, JF, 2015. Linear elastic fracture mechanics predicts the propagation distance of frictional slip. Tribol. Lett. 57.
Karner, S.L., Marone, C.J., 2000. Effects of loading rate and normal stress on stress drop and stick slip recurrence interval. GeoComplexity Phys. Earthquakes.
Leeman, J.R., Saffer, D.M., Scuderi, M.M, Marone, C., 2016. Laboratory observations of slow earthquakes and the spectrum of tectonic fault slip modes. Nat. Commun. 7, 11104. doi:10.1038/ncomms11104.
Luo, Y., Ampuero, J.-P., 2018. Stability of faults with heterogeneous friction properties and effective normal stress. Tectonophysics 733, 257–272. https://doi.org/10.1016/J.TECTO.2017.11.006.
Mair, K., Frye, K.M., Marone, C., 2002. Influence of grain characteristics on the friction of granular shear zones. J. Geophys. Res. 107 (B10), 2219. https://doi.org/10.1029/2001JB000516.
Marone, C., Vidale, J.E., Ellsworth, W.L., 1995. Fault healing inferred from time dependent variations in source properties of repeating earthquakes. Geophys. Res. Lett. https://doi.org/10.1029/95GL03076.
Marone, C., 1998a. Laboratory-derived friction laws and their application to seismic faulting. Ann. Rev. Earth Planetary Sci. 26 (1), 643–696. https://doi.org/10.1146/annurev.earth.26.1.643.
Marone, C., 1998b. The effect of loading rate on static friction and the rate of fault healing during the earthquake cycle. Nature 391 (6662), 69–72. https://doi.org/10.1038/34157.
McLaskey, G.C., Thomas, A.M., Glaser, S.D., Nadeau, R.M., 2012. Fault healing promotes high-frequency earthquakes in laboratory experiments and on natural faults. Nature 491 (7422), 101–104. https://doi.org/10.1038/nature11512.
Perfettini, H., Molinari, A., 2017. A micromechanical model of rate and state friction: 1. static and dynamic sliding. J. Geophys. Res. 122 (4), 2590–2637. https://doi.org/10.1002/2016JB013302.
Rabinowicz, E., 1951. The nature of the static and kinetic coefficients of friction. J. Appl. Physc 22, 1373–1379.
Rabinowicz, E., 1956. Stick and slip. Sci. Am. 194 (5), 109–119. doi:10.1038/scientificamerican0556-109.
Ranjith, K, Rice, JR, 1999. Stability of quasi–static slip in a single degree of freedom elastic system with rate and state dependent friction. J. Mech. Phys. Solids 47, 1207–1218.
Rice, J.R., 1993. Spatio-temporal complexity of slip on a fault. J. Geophys. Res. 98 (B6), 9885. https://doi.org/10.1029/93JB00191.
Rice, J.R., Lapusta, N., Ranjith, K., 2001. Rate and state dependent friction and the stability of sliding between elastically deformable solids. J. Mech. Phys. Solids 49 (9), 1865–1898. doi:10.1016/S0022-5096(01)00042-4.
Rice, J.R., Ruina, A.L., 1983. Stability of steady frictional slipping. J. Appl. Mech. 50 (2), 343. https://doi.org/10.1115/1.3167042.
Rice, J.R., Tse, S.T., 1986. Dynamic motion of a single degree of freedom system following a rate and state dependent friction law. J. Geophys. Res. 91 (1), 521–530.
Roy, M., Marone, C.J., 1996. Earthquake nucleation on model faults with rate and state friction: effects of inertia. J. Geophys. Res.
Ruina, A., 1983. Slip instability and state variable friction laws. J. Geophys. Res. 88, 10359–10370.
Scholz, C.H., 2002. The Mechanics of Earthquakes and Faulting. Cambridge University Press.
Scuderi, M.M., Carpenter, B.M., Johnson, P.A., Marone, C., 2015. Poro mechanics of stick–slip frictional sliding and strength recovery on tectonic faults. J. Geophys. Res. 120, 6895–6912. https://doi.org/10.1002/2015JB011983.
Singh, B.R., 1960. Study of critical velocity of stick–slip sliding. J. Eng. Ind 82 (4), 393–398. doi:10.1115/1.3664261.
Shimamoto, T., Handin, J., Logan, J.M., 1980. Specimen-apparatus interaction during stick–slip in a triaxial compression machine: a decoupled two-degree-of-freedom model. Tectonophysics 67, 175–205. doi:10.1016/0040-1951(80)90234-6.
Svetlizky, I., Bayart, E., Cohen, G., Fineberg, J., 2017. Frictional resistance within the wake of frictional rupture fronts. Phys. Rev. Lett. 118 (23), 1–5. https://doi.org/10.1103/PhysRevLett.118.234301.
Tian, K., Gosvami, N.N., Goldsby, D.L., Liu, Y., Szlufarska, I., Carpick, R.W., 2017. Load and time dependence of interfacialchemical bondinduced friction at the nanoscale. Phys. Rev. Lett. 118 (7), 076103.
Vidale, J.E., Ellsworth, W.L., Cole, A., Marone, C.J., 1994. Variations in rupture process with recurrence interval in a repeated small earthquake. Nature 368 (6472), 624–626. https://doi.org/10.1038/368624a0.